Functionally-Coupled Ion Channels Begin Co-assembling at the Start of Their Synthesis

Authors:

Roya Pournejati[1,2], Jessica M. Huang[1,2], Michael Ma[1,2], Claudia M. Moreno[2,3], Oscar Vivas[1,2*]

Affiliations:

[1] Department of Pharmacology, University of Washington

[2] Department of Neurobiology and Biophysics, University of Washington

[3] Howard Hughes Medical Institute

***Corresponding author:**

Oscar Vivas

Department of Pharmacology

Department of Neurobiology and Biophysics

University of Washington, School of Medicine

Box 357290

Seattle, WA 98195-7290

Email: vivas@uw.edu

Phone: (206) 543-0958

Summary

Calcium binding to BK channels lowers BK activation threshold, substantiating functional coupling with calcium-permeable channels. This coupling requires close proximity between different channel types, and the formation of BK–Ca_V1.3 hetero-clusters at nanometer distances exemplifies this unique organization. To investigate the structural basis of this interaction, we tested the hypothesis that BK and Ca_V1.3 channels assemble before their insertion into the plasma membrane. Our approach incorporated four strategies: (1) detecting interactions between BK and Ca_V1.3 proteins inside the cell, (2) identifying membrane compartments where intracellular hetero-clusters reside, (3) measuring the proximity of their mRNAs, and (4) assessing protein interactions at the plasma membrane during early translation. These analyses revealed that a subset of BK and Ca_V1.3 transcripts are spatially close in micro-translational complexes, and their newly synthesized proteins associate within the endoplasmic reticulum (ER) and Golgi. Comparisons with other proteins, transcripts, and randomized localization models support the conclusion that BK and Ca_V1.3 hetero-clusters form before their insertion at the plasma membrane.

Significance statement

This work examines the proximity between BK and Ca_V1.3 molecules at the level of their mRNAs and newly synthesized proteins to reveal that these channels interact early in their biogenesis. Two cell models were used: a heterologous expression system to investigate the steps of protein trafficking and a pancreatic beta cell line to study the localization of endogenous channel mRNAs. Our findings show that BK and Ca_V1.3 channels begin assembling intracellularly before reaching the plasma membrane, revealing new aspects of their spatial organization. This intracellular assembly suggests a coordinated process that contributes to functional coupling.

Introduction

This work concerns the organization of functionally coupled voltage- and calcium-dependent potassium (BK) channels and voltage-gated calcium (Ca_V) channels.

BK channels (a.k.a. K_{Ca}1.1, Maxi-K, Slo1, KCNMA1) are named for their "big potassium (K^+)" conductance, since channel opening leads to unusually large, outward potassium currents and membrane repolarization. Its amino acid sequence is conserved throughout the animal kingdom from worms to mammals. BK channels are expressed in a wide variety of cell types, predominantly excitable cells but also non-excitable salivary, bone and kidney cells, making this channel responsible for a large range of physiological processes [1-9]. Phenotypes of pathological BK mutations in human patients are most prominent in the brain and muscle and often manifest as seizures, movement disorders, developmental delay, and intellectual disability [10, 11]. BK is also implicated in other organ system functions, including but not limited to heart pace making, reproduction, and pancreatic glucose homeostasis [11, 12].

Since BK channels affect function in numerous physiological systems, channel opening is meticulously regulated at the cellular level. BK is a voltage-gated channel activated by membrane depolarization. Interestingly, BK has an additional gating mechanism that differentiates it from typical voltage-gated potassium channels; BK opening is gated by both voltage and intracellular calcium binding to a cytosolic regulatory domain. At the cytoplasmic resting free calcium concentration (~0.1 μM), BK channels remain closed [13]. However, the probability of channel opening increases when both the membrane potential depolarizes and when the local free calcium rises. Yet, increases of calcium are tightly limited by endogenous proteins that bind calcium with high affinity as well as by extrusion mechanisms that take calcium inside organelles or outside the cell. Hence, the activation of BK channels relies on strategies to overcome these regulatory barriers. One such strategy is to localize near sources of calcium.

In excitable cells, BK forms nanodomains with calcium channels that provide exclusive, localized calcium sources. Several subtypes of calcium channels form functional signaling complexes with BK, shifting BK activation voltages to more negative potentials [14-16]. One of these channels, Ca_V1.3 (a.k.a. *CACNA1D*), is unique in its electrophysiological profile as an L-type calcium channel, activating with fast kinetics at voltages as negative as -55 mV [17]. Additionally, BK channels are modulated by

Mechanism	Description	Source
Co-translation of heteromeric channel subunits	mRNA transcripts and nascent proteins of hERG heteromeric subunits form molecular complexes during protein translation.	[19]
Co-translation of channels permeating different ions	Potassium channel hERG and sodium channel SCN5A form complexes of mRNA transcripts and nascent proteins during protein translation.	[20]
Membrane curvature sensing	Clusters of Piezo1 channels enrich in membrane invaginations.	[21]
ER membrane protein complex	ER membrane complex acts as a chaperone for heteromeric channel assembly.	[22]
Scaffolding proteins	Scaffolding protein AKAP150 is required for abnormal gating of Ca_V1.2-LQT8 channels.	[23]
Random insertion	Clusters of Ca_V1.2, Ca_V1.3, BK, and TRPV4 are proposed to be randomly formed into the plasma membranes of smooth muscle, cardiac muscle, hippocampal neurons, and tsA-201 cells.	[24]

Table 1. List of mechanisms described for the interaction between channel subunits, channels of the same type (homo-clusters), or hetero-clusters of channel families permeating different ions.

auxiliary subunits, which fine-tune BK channel gating properties to adapt to different physiological conditions. β and γ subunits regulate BK channel kinetics, altering voltage sensitivity and calcium responsiveness [18]. These interactions ensure precise control over channel activity, allowing BK channels to integrate voltage and calcium signals dynamically in various cell types. Here, we focus on the selective assembly of BK channels with Ca_V1.3 and do not evaluate the contributions of auxiliary subunits to BK channel organization. Ca_V1.3 is expressed in many of the same cell types as BK and is often functionally coupled with BK channels, enabling BK channels to activate at more negative voltages. Notably, super-resolution microscopy shows that Ca_V1.3 organizes spatially into nanodomains with BK in the plasma membrane [15]. However, the mechanisms behind the assembly of BK and Ca_V1.3 hetero-clusters are unknown.

Several mechanisms for bringing ion channels together have been suggested (Table 1). One proposes that proteins assembly precedes protein insertion into the plasma membrane [19, 25, 26]. This mechanism has been observed in studies of hetero-multimers and even channels permeating different ions. The formation of these groups of proteins would start from their synthesis. There is even the possibility of mRNA transcripts colocalizing prior to translation. We explored this mechanism in relation to BK and Ca_V1.3 functional coupling. Here, we started by investigating when and where BK and Ca_V1.3 channels cluster in the cell. We looked for BK and

Ca_V1.3 hetero-clusters at intracellular membranes of the ER, at ER exit sites, and at the Golgi. We also investigated the proximity between mRNA transcripts of BK and Ca_V1.3.

Definitions used in this manuscript

To guide the reader and prevent confusion on the terms used, we introduce the following nomenclature, which is also illustrated in Figure 1. Molecular complex: an array of several polypeptides with a defined function. In our case, a BK channel is a molecular complex of four alpha subunits whose function is to permeate ions. Homo-cluster: we define a homo-cluster as the accumulation of proteins. In our work, a homo-cluster refers to the accumulation of BK channels or the accumulation of calcium channels.

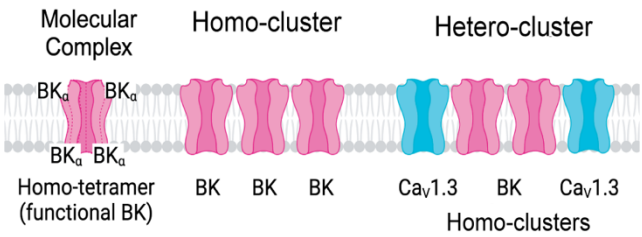

Figure 1. Representation of molecular complex, homo-cluster, and hetero-cluster.

Hetero-cluster: we define a hetero-cluster as the collection of different types of proteins that facilitate functional coupling and compartmentalization of a signaling complex. In the present work, hetero-cluster refers to a coordinated collection of BK and Ca_V channels. It is also used to refer to the assembly of homo-clusters of BK with homo-clusters of Ca_V channels.

Materials and Methods

Cell culture:

We used tsA-201 cells to co-express BK and Ca_V1.3 channels heterologously. Cells were grown in DMEM (Gibco) supplemented with 10% fetal bovine serum and 0.2% penicillin/streptomycin. We used rat insulinoma (INS-1) cells to study endogenous levels of transcripts and proteins of channels. INS-1 cells were cultured in RPMI high glutamate medium (Gibco) with 10% fetal bovine serum, 0.2% penicillin/streptomycin, 10 mM HEPES (Gibco), 1 mM sodium pyruvate (Gibco), and 50 μM 2-mercaptoethanol. Both cell types were passaged twice a week and incubated in 5% CO_2 at 37°C.

Plasmids and transfection:

Cells were transfected with 0.1– 0.4 μg DNA per plasmid and plated for 24 hours on poly-D-Lysine coated coverslips. Lipofectamine 3000 (Invitrogen, RRID: L30000) was used for the transfection. DNA clones of Ca_V1.3, BK channels, PH-PLCδ GFP, ER moxGFP, pmGFP-Sec16S and Golgi-mGFP were obtained from Addgene (RRID:SCR_002037). The Ca_V1.3 α subunit construct used in our study corresponds to the rat Ca_V1.3e splice variant containing

exons 8a, 11, 31b, and 42a, with a deletion of exon 32. The BK channel construct corresponds to the VYR splice variant of the mouse BKα subunit (KCNMA1). Auxiliary subunits for Ca_V1.3 channels, Ca_Vβ3 and Ca_Vα2δ1 (from Diane Lipscombe, Brown University, RI), were transfected as well. No BK channel auxiliary subunits were transfected.

Antibodies:

Ca_V1.3 channels were immuno-detected with a rabbit primary antibody recognizing residues 809 to 825 located at the intracellular II-III loop of the channel (DNKVTIDDYQEEAEDKD), kindly provided by Drs. William Catterall and Ruth Westenbroek [27]. BK channels were detected using the anti-Slo1 mouse monoclonal antibody clone L6/60. The goat polyclonal GFP antibody was against the recombinant full-length protein corresponding to *Aequorea victoria* GFP. Anti-58K Golgi protein antibody was used to mark the Golgi. Specificity of antibodies was tested in un-transfected tsA-201 cells (Figure 2- Supplementary 1). The secondary antibodies tagged with Alexa dyes were Donkey anti-mouse Alexa-647, Donkey anti-rabbit Alexa-555, Donkey anti-goat Alexa-488 (Molecular Probes).

Immunostaining:

Cells were fixed with freshly prepared 4% paraformaldehyde for 10 minutes. After washing, aldehydes were reduced with 0.1% $NaBH_4$ for 5 minutes and then washed again. Nonspecific binding was blocked with 3% bovine serum albumin (Thermo Scientific). Cells were permeabilized with 0.25% v/v Triton X-100 in PBS for 1 hour. Primary antibodies were used at 10 µg/ml in blocking solution and incubated overnight at 4°C. After washing, secondary antibodies at 2 µg/ml were incubated for 1 hour at 21˚C. Washing steps indicated in all methods include 3 cycles of rinsing and rocking for 5 minutes with PBS at 21˚C. Cells were imaged using an inverted AiryScan microscope or an ONI Nanoimager with super-resolution capabilities, in total internal reflection fluorescence (TIRF) mode, and with a Z-resolution of 50 nm.

Proximity ligation assay (PLA):

Cells were fixed with freshly prepared 4% paraformaldehyde for 10 minutes. After washing, aldehydes were reduced with 50 mM glycine for 15 minutes. After another round of washes, PLA was performed according to manufacturer instructions (Duolink® In Situ Red Starter Kit). Cells were blocked and permeabilized with Duolink blocking solution. Primary antibodies were used at 10 µg/ml in Duolink antibody diluent and incubated overnight at 4°C. The

Duolink® In Situ PLA® probe anti-rabbit PLUS and anti-mouse MINUS were used as secondary antibodies, followed by ligation and amplification. For PLA combined with immunostaining, PLA was followed by a secondary antibody incubation with Alexa Fluor-488 at 2 µg/ml for 1 hour at 21˚C. Since GFP fluorescence fades significantly during the PLA protocol, resulting in reduced signal intensity and poor image resolution, GFP was labeled using an antibody rather than relying on its intrinsic fluorescence. Coverslips were mounted using ProLong™ Gold Antifade Mountant with DAPI. Cells were imaged using an inverted Zeiss AiryScan microscope.

Single-molecule fluorescence in situ hybridization (RNAscope™):

Manual RNAscope assay was performed using RNAscope Multiplex Fluorescent V2 Assay according to the manufacturer's protocol. The RNAscope assay consists of target probes and a signal amplification system composed of a preamplifier, amplifier, and label probe. A schematic RNAscope assay procedure is shown in Figure 5- Supplementary 1. Briefly, cells were fixed with 4% paraformaldehyde for 30 minutes, washed, dehydrated, and then rehydrated with ethanol, and permeabilized with 0.1% Tween-20 in PBS. Next, cells were quenched with H_2O_2 and treated with Protease III. Probes were hybridized for 2 hours at 40°C followed by RNAscope amplification and then fluorescence detection. Coverslips were mounted using ProLong™ Gold Antifade Mountant with DAPI. We used the following RNAscope probes: RNAscope 3-plex Positive Control Probes, RNAscope 3-plex negative control probes, RNAscope™ Probe- Rn-Ryr, RNAscope™ Probe- Rn-Scn9a, RNAscope Probe- Rn-Kcnma1-C3, RNAscope Probe- Rn-Cacna1d-C2, and RNAscope Probe- Rn-Gapdh. Cells were imaged on the inverted AiryScan microscope. For PLA and RNAscope experiments, we used custom-made macros written in ImageJ. Processing of PLA data included background subtraction. To assess colocalization, fluorescent signals were converted into binary images, and channels were multiplied to identify spatial overlap. Specificity of RNAscope probes was tested in un-transfected tsA-201 cells (Figure 5-Supplementary 2). For RNAscope combined with immunostaining, RNAscope was followed by blocking in PBS supplemented with 0.01 % Tween-20 and 3% BSA for 1 h at 21˚C. Samples were then probed for BK protein using primary antibody overnight at 4˚C followed by secondary antibody incubation with Alexa Fluor-488 at 2 µg/ml for 1 hour at 21˚C. Coverslips were mounted using ProLong™ Gold Antifade Mountant. Cells were imaged using an inverted Zeiss AiryScan microscope.

High resolution imaging:

Cells were imaged using an inverted AiryScan microscope (Zeiss LSM 880) run by ZEN black v2.3 software and equipped with a plan apochromat 63X oil immersion objective with 1.4 NA. Fluorescent dyes were excited with a 405 nm diode, 458–514 nm argon, 561 nm, or 633 nm laser. Emission light was detected using an Airyscan 32 GaAsP detector and appropriate emission filter sets. The point spread functions were calculated using ZEN black software and 0.1 µm fluorescent microspheres. The temperature inside the microscope housing was 22°C. Images were analyzed using ImageJ (NIH).

Super-resolution imaging:

Direct stochastic optical reconstruction microscopy (dSTORM) images of BK and Ca_V1.3 overexpressed in tsA-201 cells were acquired using an ONI Nanoimager microscope equipped with a 100X oil immersion objective (1.4 NA), an XYZ closed-loop piezo 736 stage, and triple emission channels split at 488, 555, and 640 nm. Samples were imaged at 35°C. For single-molecule localization microscopy, fixed and stained cells were imaged in GLOX imaging buffer containing 10 mM β-mercaptoethylamine (MEA), 0.56 mg/ml glucose oxidase, 34 µg/ml catalase, and 10% w/v glucose in Tris-HCl buffer. Single-molecule localizations were filtered using NImOS software (v.1.18.3, ONI). Localization maps were exported as TIFF images with a pixel size of 5 nm. Maps were further processed in ImageJ (NIH) by thresholding and binarization to isolate labeled structures. To assess colocalization between the signal from two proteins, binary images were multiplied. Particles smaller than 400 nm^2 were excluded from the analysis to reflect the spatial resolution limit of STORM imaging (20 nm) and the average size of BK channels. To examine spatial localization preference, binary images of BK were progressively dilated to 20 nm, 40 nm, 60 nm, 80 nm, 100 nm, and 200 nm to expand their spatial representation. These modified images were then multiplied with the Ca_V1.3 channel to quantify colocalization and determine BK occupancy at increasing distances from Ca_V1.3. To ensure consistent comparisons across distance thresholds, data were normalized using the 200 nm measurement as the highest reference value, set to 1.

Image scrambling:

Images were binarized as TIFF images, and their respective cell perimeter coordinates were exported as CSV files by ImageJ. Processed binary images were then analyzed by our SpotScrambler (https://github.com/jehuang2/SpotScrambler) Python program. SpotScrambler first extracts the areas of fluorescent particles in

the binary image. SpotScrambler then redraws the fluorescent particles as circles at randomized coordinates within cell perimeter boundaries. SpotScrambler accurately preserves particle number and particle sizes, averaging less than 1% difference in total area of fluorescent particles between pre-SpotScrambler and post-SpotScrambler images. To ensure reliable randomization for each experiment, results were averaged between 3 trials of SpotScrambler.

Data analysis

Excel (Microsoft), and Prism (GraphPad) were used to analyze data. ImageJ was used to process images. One-way ANOVA and non-parametric statistical test (Mann-Whitney Wilcoxon) were used to test for statistical significance. p-values <0.05 were deemed statistically significant. The number of cells used for each experiment is detailed in each figure legend.

Results

BK and Ca_V1.3 hetero-clusters are found inside the cell.

BK and Ca_V hetero-clusters have been observed at the plasma membrane [14-16]. However, a clear understanding of when or how BK and Ca_V hetero-clusters assemble is missing. A simple mechanism proposes that these hetero-clusters organize only at the plasma membrane. Here, we tested the alternative hypothesis of BK and Ca_V assembling inside the cell (Figure 2A). To test this idea, we used proximity ligation assay (PLA) and antibodies against BK and Ca_V1.3 channels. When these antibodies are within 40 nm of each other, PLA ligation and amplification can occur, resulting in the formation of fluorescent puncta (Figure 2B), here referred to as PLA puncta. Hence, the PLA puncta in Figure 2C represent BK and Ca_V1.3 hetero-clusters. To confirm specificity, a negative control was performed by probing only for BK using the primary antibody, ensuring that detected signals were not due to non-specific binding or background fluorescence. We first analyzed Z-projections, in which all the puncta in the cell volume are added, and found a density of 5.8 ± 1.0 / 10 μm^2. In a different experiment, we analyzed the puncta density for each focal plane of the cell (step size of 300 nm) and compared the puncta at the plasma membrane to the rest of the cell. We visualized the plasma membrane with a biological sensor tagged with GFP (PH-PLCδ-GFP) and then probed it with an antibody against GFP (Figure 2E). By analyzing the GFP signal, we created a mask that represented the plasma membrane. The mask served to distinguish between the PLA puncta located inside the cell and those at the plasma membrane, allowing us to calculate the number of PLA puncta at the plasma membrane. To our surprise, we

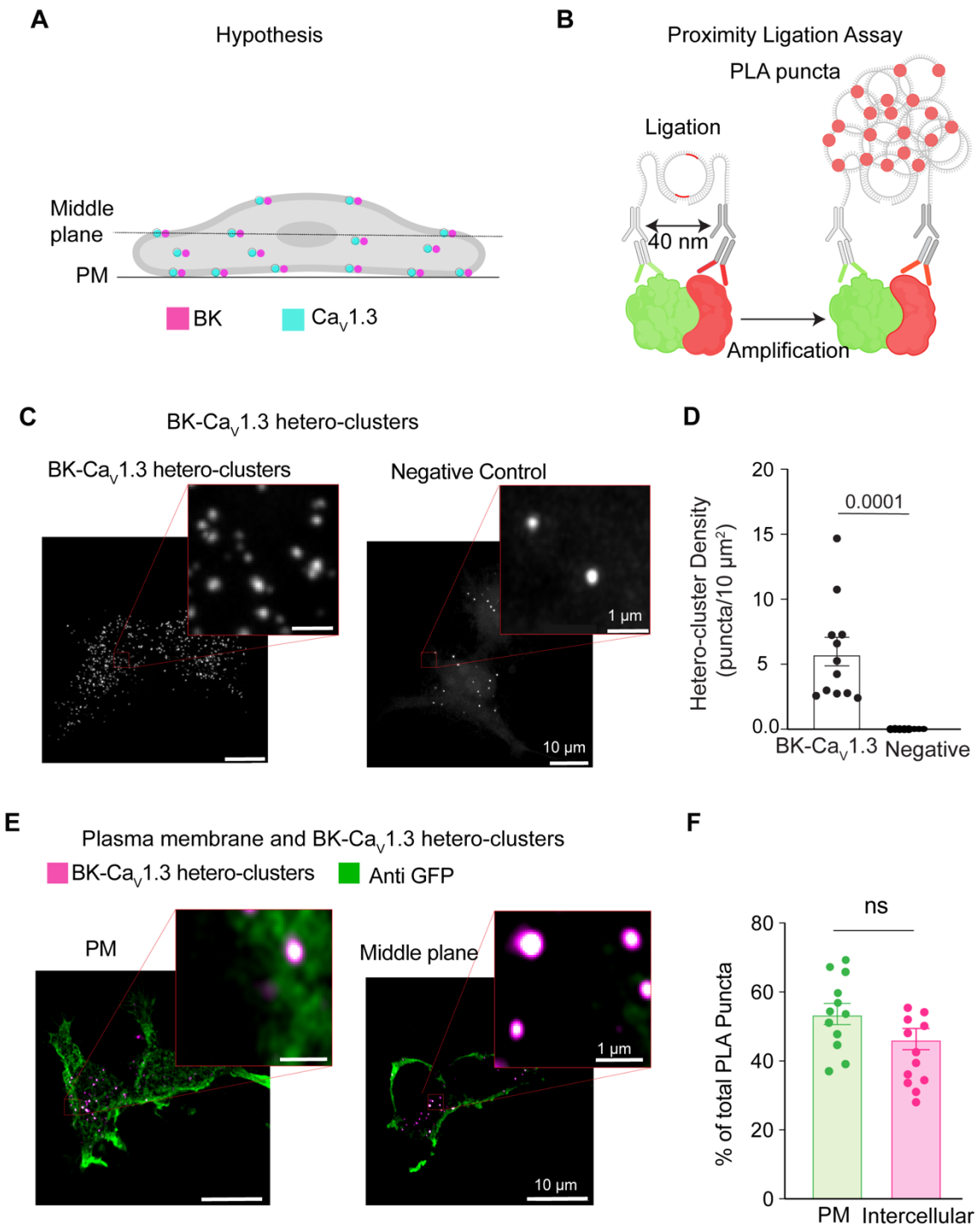

Figure 2. BK and Ca$_V$1.3 hetero-clusters are found inside the cell. A. Diagram of the hypothesis: hetero-clusters of BK (magenta) and Ca$_V$1.3 (cyan) are on intracellular membranes and on the plasma membrane. **B.** Illustration of the technique to detect BK and Ca$_V$1.3 hetero-clusters. Proximity ligation assay is used to detect the hetero-clusters. **C.** Confocal images of fluorescent puncta from PLA experiments in tsA-201 cells. Left: Cells were transfected and probed for BK and Ca$_V$1.3 channels. Right: negative control. Cells were transfected and probed only for BK channels. Enlargement of a selected region is shown in the inset. **D.** Scatter dot plot comparing puncta density of BK and Ca$_V$1.3 hetero-clusters to the negative control. Data points are from n = 12 cells for BK and Ca$_V$1.3 hetero-clusters and from n = 14 cells for negative control. *p*-values are shown at the top of the graphs. **E.** Confocal images of fluorescent PLA puncta at different focal planes co-labeled against GFP at the plasma membrane. Cells were transfected with BK, Ca$_V$1.3, and PH-PLCδ-GFP and probed for BK channels, Ca$_V$1.3 channels, and GFP. PLA puncta are shown in magenta, and the plasma membrane is shown in green. Enlargements of the representative regions of PM and intercellular hetero-clusters are shown in the insets. **F.** Scatter dot plot comparing BK and Ca$_V$1.3 hetero-cluster abundance at PM and inside the cell. Data points are from n = 12 cells. Scale bar is 10 µm and 1 µm in the insets.

found a significant number of puncta localized inside the cell. 46 ± 3 % of the puncta were localized intracellularly, whereas 54 ± 3 % were at the plasma membrane. This finding is consistent with our supposition that BK and Ca_V1.3 channels colocalize in the cell.

BK and Ca_V1.3 hetero-clusters localize at ER and ER exit sites.

We next investigated the identity of the intracellular membranes where these PLA puncta were found. A large component of intracellular membranes in the cell is the endoplasmic reticulum (ER), where channels are inserted after translation. To determine whether BK and Ca_V1.3 associate in the ER (Figure 3A), we combined PLA with immunodetection. As before, PLA probed for BK and Ca_V1.3 hetero-clusters, while a KDEL-moxGFP label identified the ER (Figure 3B). To avoid disruption of organelle architecture, we used the monomeric mox version of KDEL-GFP, which is optimized to reduce oligomerization in the ER environment [28]. Neither overexpression of KDEL-moxGFP nor fixation altered the ER structure as the tubule width remained around 150 nm for either condition (Figure 3C), a value in agreement with the literature [29, 30]. To assess the percentage of PLA puncta colocalizing with the ER, we employed two different cell lines, our overexpression system (tsA-201 cells) and a rat insulinoma cell line (INS-1) that expresses BK and Ca_V1.3 channels endogenously. In this and following experiments, we analyze one focal plane, in the middle of the cell, to quantify PLA puncta colocalization with ER membrane. Figure 3D shows PLA puncta in the same space as the ER. Comparing the overexpression and endogenous systems, 63 ± 3% versus 50 ± 6% of total PLA puncta were localized at the ER (Figure 3E). To determine whether the observed colocalization between BK–Ca_V1.3 hetero-clusters and the ER was not simply due to the extensive spatial coverage of ER labeling, we labeled ER exit sites using Sec16-GFP and probed for hetero-clusters with PLA. This approach enabled us to test whether the hetero-clusters were preferentially localized to ER exit sites, which are specialized trafficking hubs that mediate cargo selection and direct proteins from the ER into the secretory pathway. In contrast to the more expansive ER network, which supports protein synthesis and folding, ER exit sites ensure efficient and selective export of proteins to their target destinations.

By quantifying the proportion of BK and Ca_V1.3 hetero-clusters relative to total channel expression at ER exit sites, we found 28 ± 3% colocalization in tsA-201 cells and 11 ± 2% in INS-1 cells (Figure 3F). While the percentage of colocalization between hetero-clusters and the ER or ER exit sites

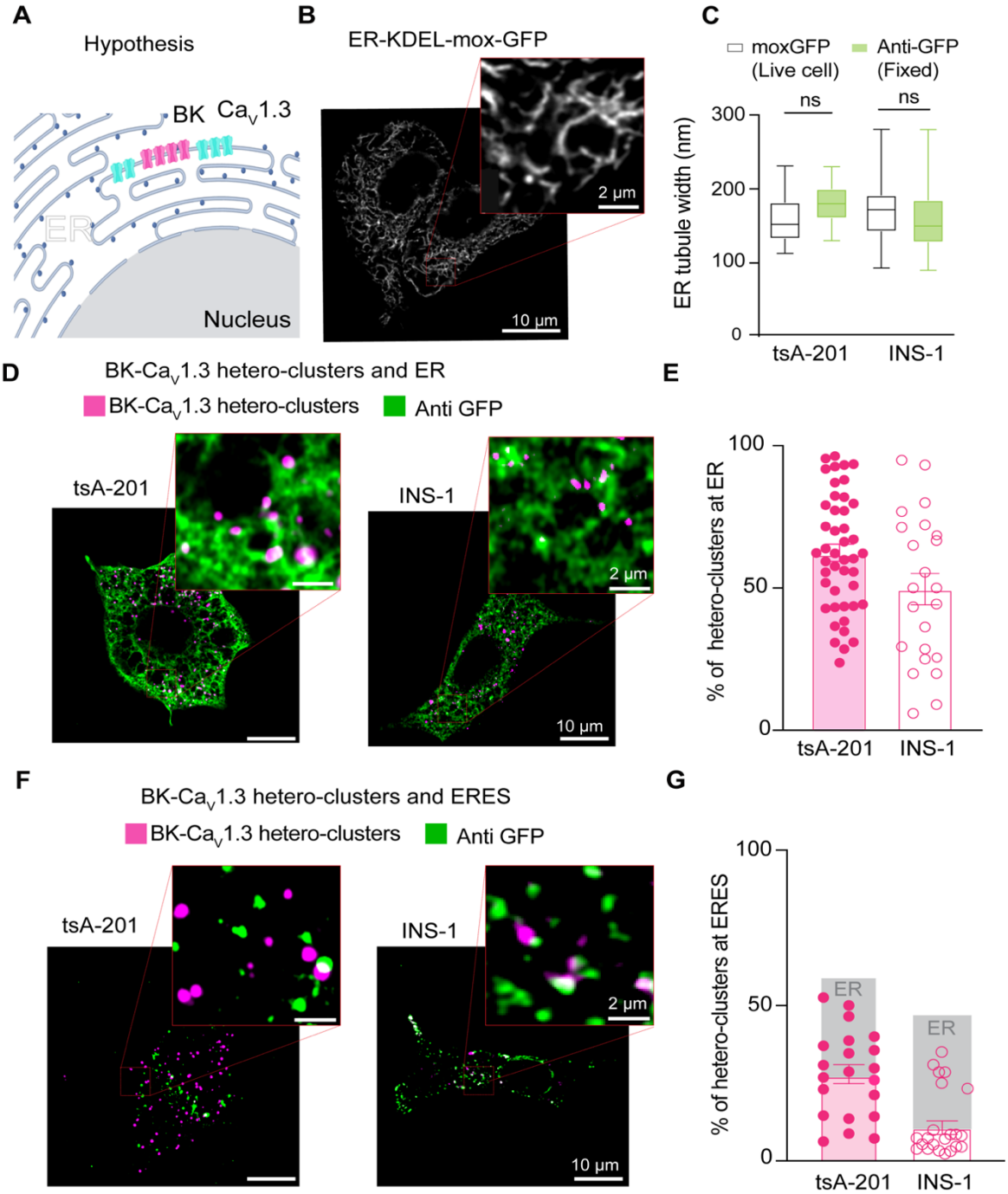

Figure 3. BK and Ca$_V$1.3 hetero-clusters localize at ER and ER exit sites (ERES). A. Diagram of the hypothesis: hetero-clusters of BK (magenta) and Ca$_V$1.3 (cyan) can be found at the ER membrane. **B.** Representative image of the ER labeled with exogenous GFP in INS-1 cells. Cells were transfected with KDEL-moxGFP. Magnification is shown in the inset. **C.** Comparison of the ER tubule distance in live and fixed tsA-201 and INS-1 cells. Data points are from n = 23 tsA-201 cells, n = 27 INS-1 cells **D.** Representative images of PLA puncta and ER. Left: tsA-201 cells were transfected with BK, Ca$_V$1.3 and KDEL-moxGFP. Right: INS-1 cells were transfected only with KDEL-moxGFP. Fixed cells were probed for BK-Ca$_V$1.3 hetero-clusters (PLA puncta) and GFP. PLA puncta is shown in magenta. ER is shown in green. **E.** Comparison of BK-Ca$_V$1.3 hetero-clusters found at the ER and relative to all PLA puncta in the cell. Values are given in percentages. **F.** Representative images of PLA puncta and ER exit sites. Left and right are the same as in D, but cells were transfected with Sec16-GFP instead of KDEL. **G.** Comparison of BK-Ca$_V$1.3 hetero-clusters found at ER exit sites relative to all PLA puncta in the cell. Values are given in percentages. Data points are from n = 45 tsA-201 cells for ER, n = 21 tsA-201 cells for ERES, n = 23 INS-1 cells for ER, and n = 23 INS-1 cells for ER exit sites. Scale bar is 10 µm and 2 µm in the magnifications.

alone cannot be directly compared to infer trafficking dynamics, these findings reinforce the conclusion that hetero-clusters reside within the ER and suggest that BK and Ca_V1.3 channels traffic together through the ER and exit in coordination.

BK and Ca_V1.3 hetero-clusters go through the Golgi.

Channels are modified in the Golgi after synthesis (Figure 4A), so we asked whether PLA puncta formed by BK and Ca_V1.3 hetero-clusters can be found in the Golgi. Using the same strategy, we labeled Golgi with Gal-T-mEGFP (Figure 4B) and detected BK-Ca_V1.3 hetero-clusters using PLA. To confirm that the overexpressed Gal-T-mEGFP labels the Golgi specifically without altering its structure, we compared the region detected by the antibody against GFP to the region detected by a primary antibody against the Golgi protein 58K (Figure 4C). 58K is a specific peripheral protein that localizes to the cytosolic face of Golgi [31]. The overlay shows that the GFP signal labels the same region as the antibody against 58K. When assessing the presence of BK-Ca_V1.3 hetero-clusters in the Golgi, we found that 31 ± 5% of PLA puncta were localized at the Golgi in the overexpression system and 25 ± 4% in the endogenous cell model (Figure 4E).

We performed controls to confirm that the formation of hetero-clusters between the two channels was not coincidental but rather the result of structural coupling. We tested the formation of PLA puncta between BK channels and the Golgi protein 58K. We also tested for Ca_V1.3 and 58K. We did not find PLA puncta when the proximity between the channels and 58K was probed (Figure 4F), supporting the idea that PLA puncta between BK and Ca_V1.3 channels found at the Golgi represent specific coupling. We selected the Golgi as a control because it represents the final stage of protein trafficking, ensuring that hetero-cluster interactions observed at this point reflect specificity maintained throughout earlier trafficking steps, including within the ER.

It is important to clarify that the percentages provided in this work cannot be added up to understand the distribution of hetero-clusters along the biosynthetic pathway of the channels. The percentage in each membrane compartment was compared to the total percentage of hetero-clusters observed in each cell for that particular experiment. Therefore, there is expected overlap between our measurements due to (1) optical resolution and (2) the effect of not comparing all the organelles in the same cell. Considering these limitations, we interpreted our results as follows: about one half of hetero-clusters are found inside the cell. The other half corresponds to hetero-clusters at the plasma membrane. From the half inside the cell,

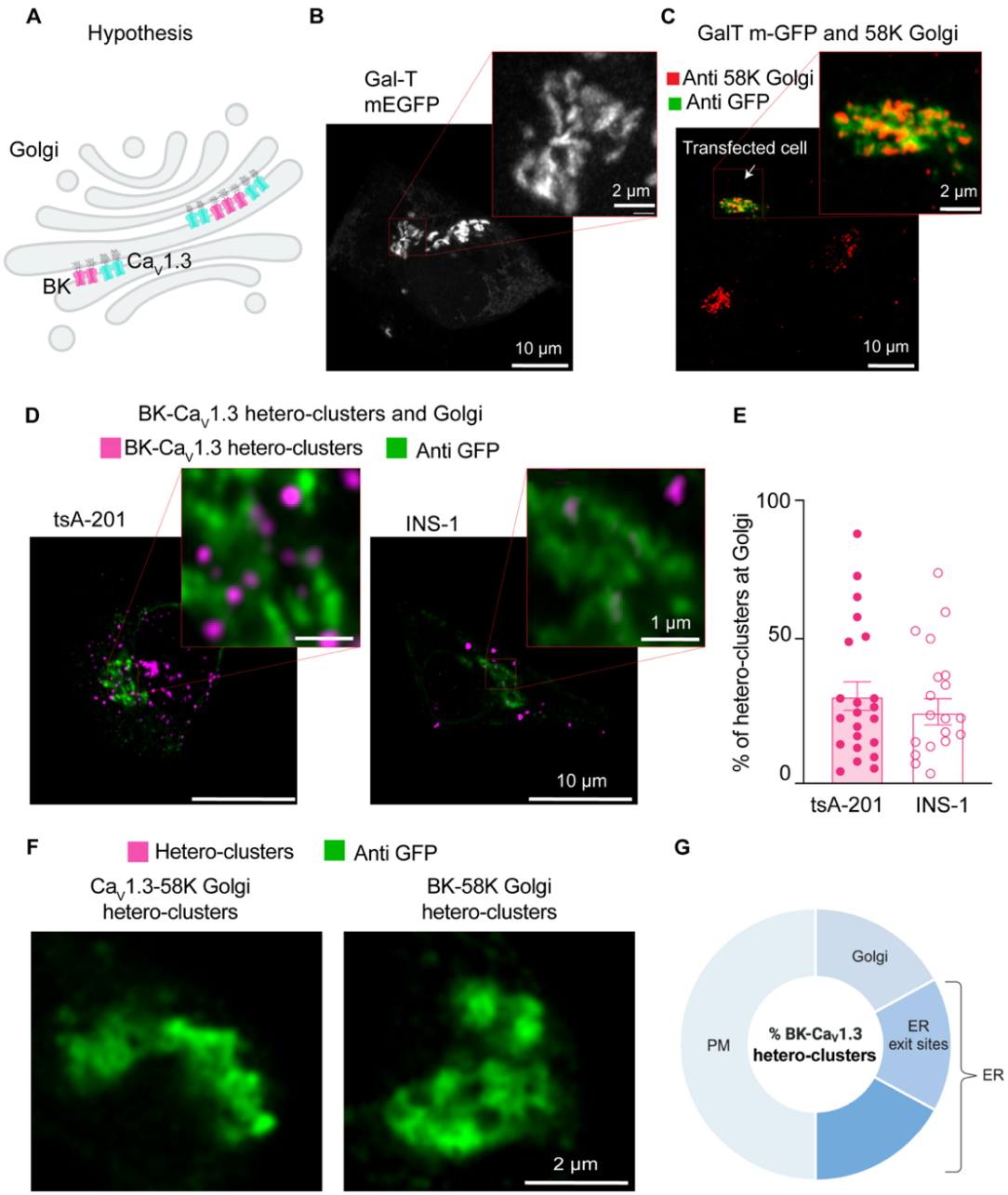

Figure 4. BK and Ca$_V$1.3 hetero-clusters go through the Golgi. A. Diagram of the hypothesis: PLA puncta detecting hetero-clusters between BK (magenta) and Ca$_V$1.3 (cyan) channels can be found at the Golgi membrane. **B.** Representative image of the Golgi structure with exogenous GFP in INS-1 cells. Cells were transfected with Gal-T-mEGFP. Enlargement is shown in the inset. **C.** Representative images of fixed cells co-stained with antibodies against Gal-T-mEGFP in green and 58K-Golgi in red **D.** Representative images of PLA puncta and Golgi. tsA-201 cells were transfected with BK, Ca$_V$1.3 and Gal-T-mEGFP (left), and INS-1 cells were transfected only with Gal-T-mEGFP (right). PLA puncta are shown in magenta. Golgi is shown in green. **E.** Scatter dot plot of percentages of BK-Ca$_V$1.3 hetero-clusters found at the Golgi relative to all PLA puncta in tsA-201 and INS1 cells. Data points are from n = 22 tsA-201 cells and n = 19 INS-1 cells. **F.** Representative image of PLA puncta and Golgi. tsA-201 cells were transfected with BK, Ca$_V$1.3, and Gal-T-mEGFP. Left: PLA was done against BK and 58K Golgi (magenta), and Golgi is shown in green. Right: PLA was done against Ca$_V$1.3 and 58K Golgi (magenta), and Golgi is shown in green. **G.** Diagram illustrating our interpretation of percentages of BK-Ca$_V$1.3 hetero-clusters found in the cell. This illustration is based on results shown in Figures 1-4. Percentages were modified to represent overlap of fluorescent signals and limited resolution. We also show that hetero-clusters found in the ER exit sites (ERES) are also accounted in the ER. Scale bars: 10 µm and 2 µm in panels B and C; 10 µm and 1 µm in panel D; 2 µm in panel F.

roughly one third of hetero-clusters is found in the Golgi, and another third is found in ER exit sites (Figure 4G). The remaining hetero-clusters are found in other regions of the ER and in membranes that we did not probe, such as vesicles. Finally, a key limitation of this approach is that we cannot quantify the proportion of total BK or Ca$_V$1.3 channels engaged in hetero-clusters within each compartment. The PLA method provides proximity-based detection, which reflects relative localization rather than absolute channel abundance within individual organelles.

BK mRNA and Ca$_V$1.3 mRNA colocalize.

How is it that BK and Ca$_V$1.3 proteins come in close proximity in membranes of the ER, ER exit sites and the Golgi? To explore the origins of the initial association, we hypothesized that the two proteins are translated near each other, which could be

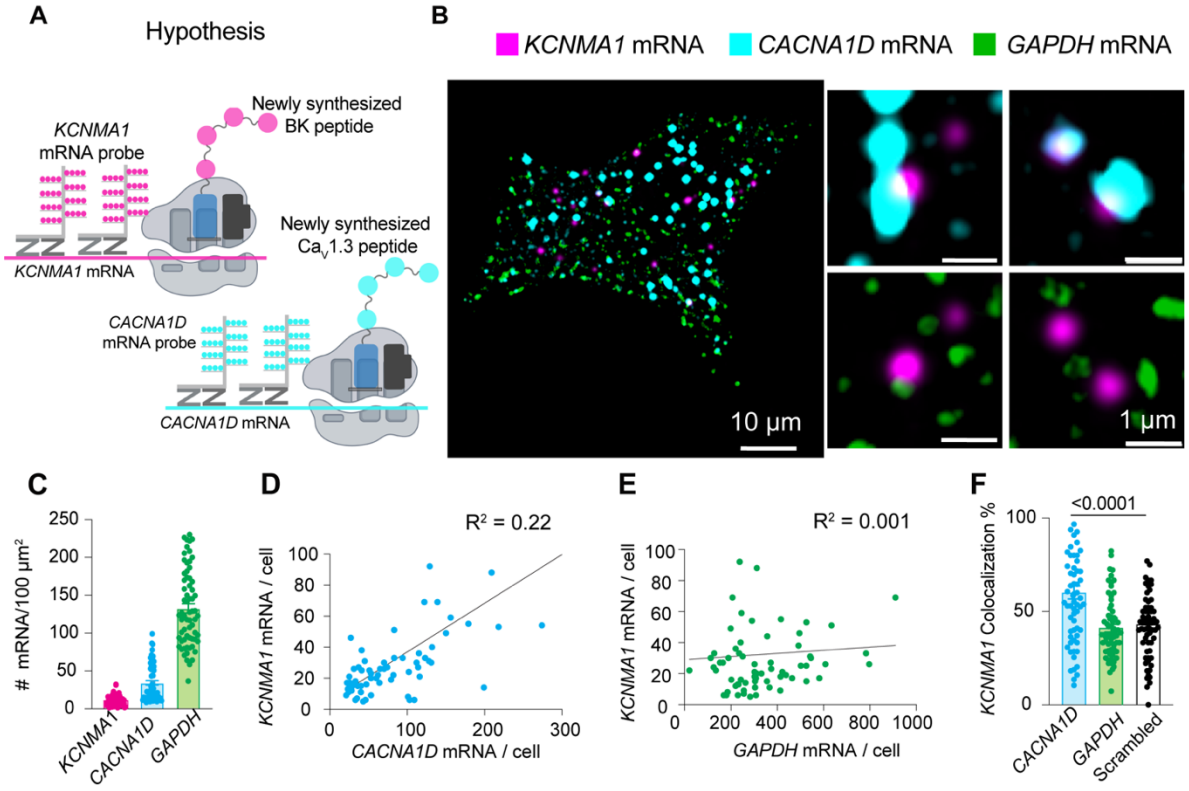

Figure 5. BK mRNA (*KCNMA1*) and Ca$_V$1.3 mRNA (*CACNA1D*) colocalize. A. Diagram of the hypothesis: *KCNMA1* and *CACNA1D* mRNAs are found in close proximity to be translated in the same neighborhood. **B.** Images of fluorescent puncta from RNA scope experiments showing *KCNMA1* mRNA in magenta, *CACNA1D* mRNA in cyan, and *GAPDH* mRNA in green. Right, magnification of three ROI. **C.** Comparison of mRNA density of *KCNMA1*, *CACNA1D*, and *GAPDH*. **D.** Correlation plot of mRNA abundance of *KCNMA1* and *CACNA1D* per cell. **E.** Correlation plot of mRNA abundance of *KCNMA1* and *GAPDH* per cell. **F.** Comparison of colocalization between *KCNMA1* mRNA and mRNA from *CACNA1D*, *GAPDH*, and scrambled images of *CACNA1D*. Data points are from n = 67 cells. Scale bar is 10 µm and 1 µm in the magnifications.

detected as the colocalization of their mRNAs (Figure 5A and B). The experiment was designed to detect single mRNA molecules from INS-1 cells in culture. We performed multiplex in situ hybridization experiments using an RNAscope fluorescence detection kit to be able to image three mRNAs simultaneously in the same cell and acquired the images in a confocal microscope with high resolution. To rigorously assess the specificity of this potential mRNA-level organization, we used multiple internal controls. *GAPDH* mRNA, a highly expressed housekeeping gene with no known spatial coordination with channel mRNAs, served as a baseline control for nonspecific colocalization due to transcript abundance. To evaluate whether the spatial proximity between BK mRNA (*KCNMA1*) and Ca_V1.3 mRNA (*CACNA1D*) was unique to functionally coupled channels, we also tested for Na_V1.7 mRNA (*SCN9A)*, a transmembrane sodium channel expressed in INS-1 cells but not functionally associated with BK. This allowed us to determine whether the observed colocalization reflected a specific biological relationship rather than shared expression context. Finally, to test whether this proximity might extend to other calcium sources relevant to BK activation, we probed the mRNA of ryanodine receptor 2 (*RyR2*), another Ca^{2+} channel known to interact structurally with BK channels [32]. Together, these controls were chosen to distinguish specific mRNA colocalization patterns from random spatial proximity, shared subcellular distribution, or gene expression level artifacts. Figure 5-Supplementary-2 shows images completely void of fluorescent signal from INS-1 cells probed for bacterial mRNA (negative control, Figure 5- Supplementary 2A) and shows images of INS-1 cells probed for mammalian mRNAs expected to be in these cells (positive control, Figure 5- Supplementary 2B). The probes against the mRNAs of interest and tested in this work were designed by Advanced Cell Diagnostics. We confirmed the specificity of the probes by performing in situ hybridization against *KCNMA1*, *CACNA1D*, *RyR2*, and *SCN9A* in non-transfected cell lines (Figure 5-Supplementary 2C and D).

Probes against *GAPDH* mRNA were used as a control in the same cells that we probed for *KCNMA1* and *CACNA1D* using the multiplex capability of this design. Transcripts were detected at different expression levels. *GAPDH* and *CACNA1D* mRNAs were more abundant (134 and 33 mRNA/100 μm^2, respectively) than *KCNMA1* mRNA (12 mRNA/100 μm^2, Figure 5C). Interestingly, the abundance of *KCNMA1* transcripts correlated more with the abundance of *CACNA1D* transcripts than with the abundance of *GAPDH*, though with a modest R^2 value (Figure 5D and E). Furthermore, *KCNMA1* and *CACNA1D*

mRNA colocalized by 60 ± 4%, which was 20% more than with *GAPDH* mRNA (Figure 5F). As an additional control and to rule out the potential influence of difference between *CACNA1D* and *KCNMA*1 abundance, we assessed *CACNA1D* colocalization against randomized, computer-generated *KCNMA1* mRNA signals, where localization was randomized while maintaining the same overall transcript count. The significantly lower (20%) colocalization observed in scrambled conditions compared to genuine BK-Cav1.3 mRNA interactions confirms that proximity is not an artifact of expression levels but reflects a specific spatial association. These results suggest that some fraction of mRNAs for BK and Ca$_V$1.3 channels are translated nearby, so the channel proteins potentially could be inserted into the same regions of the ER. We suggest that the newly synthesized proteins remain together during trafficking through the ER and the Golgi.

Next, we compared the proximity between *KCNMA1* and *SCN9A*. We detected *SCN9A* in the same cells where *KCNMA1* was found (Figure 6A). The colocalization between *KCNMA1* and *SCN9A* was only 18

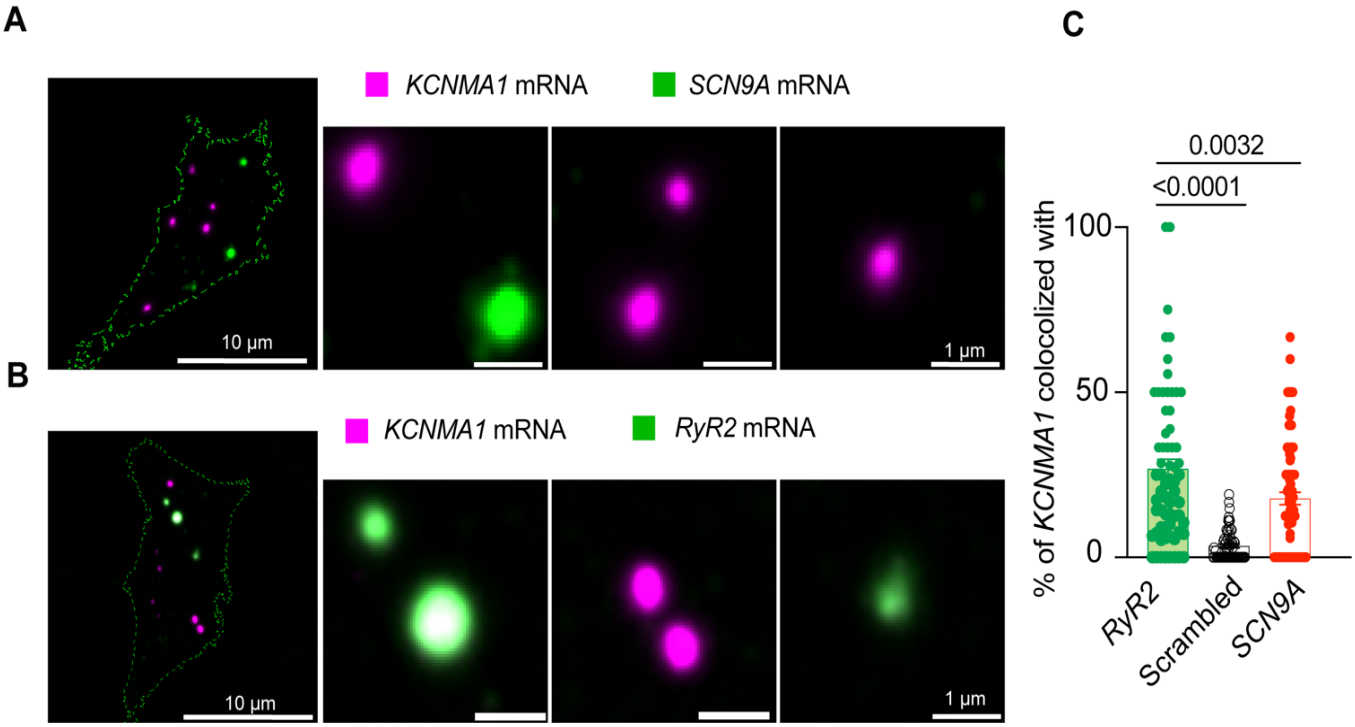

Figure 6. BK mRNA (*KCNMA1*) and RyR-2 mRNA (*RyR2*) colocalize. A. Representative confocal images of *KCNMA1* and Na$_V$1.7 (*SCN9A*) mRNA. **B.** Representative images of *KCNMA1* and *RyR2* mRNA. **C**. Comparison of the colocalization between *KCNMA1* mRNA and mRNA from *RyR2*, *SCN9A*, and scrambled images of *KCNMA1*. Data points are from n =67 cells. One way ANOVA. Scale bar is 10 µm and 1 µm in the magnifications.

± 2% (Figure 6C), which was less than what was observed with *KCNMA1* and *CACNA1D* (60%, Figure 5F). This result shows that *KCNMA1* tends to localize closer to *CACNA1D* than to *SCN9A* or *GAPDH*, supporting the specificity of *KCNMA1* and *CACNA1D* mRNA association.

With the goal of understanding if this concept could apply to other channels, we used the same approach to test a second protein known to provide calcium for BK channel opening. Similar to the coupling between BK and Ca_V1.3 channels, RyR2 also can be structurally coupled to BK channels [32]. Figure 6B shows high resolution images of single molecule in situ hybridization for *RyR2* probed together with *KCNMA1* in INS-1 cells. In the same population of cells, *KCNMA1* and *RyR2* colocalization was 27 ± 3%, which is 1.5 times that with *SCN9A* mRNA. We also assessed *RyR2* colocalization with randomized, computer-generated *KCNMA1* mRNA signals. We found that colocalization between randomized *KCNMA1* and genuine *RyR2* was 87% less colocalized compared to the analysis of genuine *KCNMA1* and genuine *RyR2* (Figure 6C), suggesting that *KCNMA1* not only colocalizes with *CACNA1D* but also with mRNA of other known calcium sources.

To further investigate whether *KCNMA1* and *CACNA1D* are localized in regions of active translation (Figure 7A), we performed RNAscope targeting *KCNMA1* and *CACNA1D* alongside immunostaining for BK protein. This strategy enabled us to visualize transcript-protein colocalization in INS-1 cells with subcellular resolution. By directly evaluating sites of active BK translation, we aimed to determine whether newly synthesized BK protein colocalized with *CACNA1D* mRNA signals (Figure 7A). Confocal imaging revealed distinct micro-translational complex where *KCNMA1* mRNA puncta overlapped with BK protein signals and were located adjacent to *CACNA1D* mRNA (Figure 7B). Quantitative analysis showed that 71 ± 3% of all *KCNMA1* colocalized with BK protein signal which means that they are in active translation. Interestingly, 69 ± 3% of the *KCNMA1* in active translation colocalized with *CACNA1D* (Figure 7C), supporting the existence of functional micro-translational complexes between BK and Ca_V1.3 channels.

BK and Ca_V1.3 channels form hetero-clusters at the plasma membrane of INS-1 cells.

We previously showed the organization of BK and Ca_V1.3 channels in hetero-clusters in tsA-201 cells and neurons, including hippocampal and sympathetic motor neurons [33]. Our present study utilizes INS-1 cells. We detected single molecules from BK and Ca_V1.3 channels in INS-1 cells using super-resolution

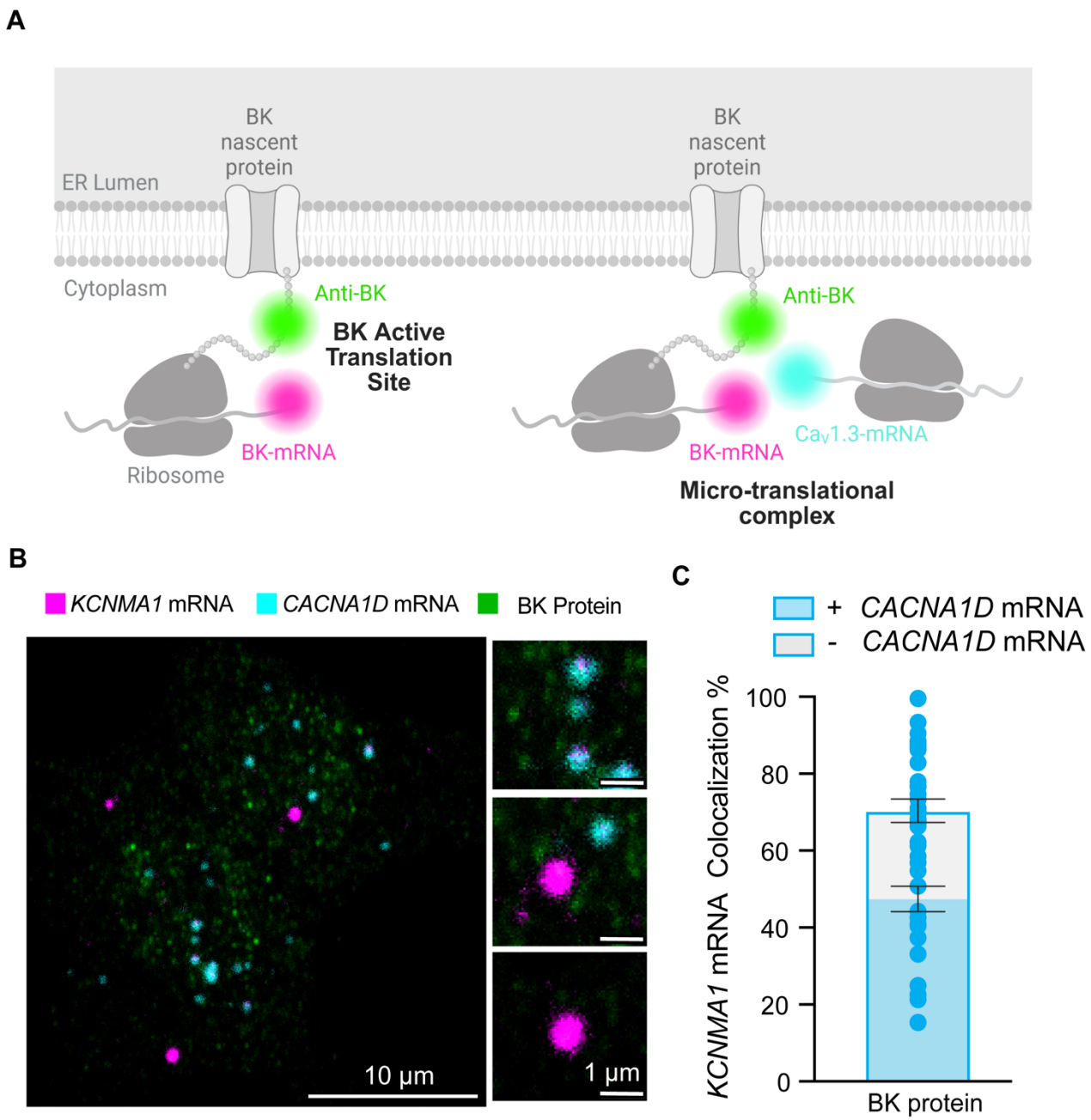

Figure 7. BK mRNA (*KCNMA1*) and Ca$_V$1.3 mRNA (*CACNA1D)* colocalize in micro-translational complexes. A. Diagram of the hypothesis: *KCNMA1* mRNAs are found in micro-translational complexes. **B.** Representative images of *KCNMA1* mRNA in magenta, *CACNA1D* mRNA in cyan, and BK protein in green. **C**. Comparison of the frequency of colocalization *KCNMA1* mRNA in active translation and in micro-translational complexes. Data points are from n = 57 cells. One way ANOVA was used as statistical analysis. Scale bar is 10 µm and 1 µm in the magnifications.

microscopy and determined their degree of colocalization. Figure 8A shows a representative image of the localizations of antibodies against BK and Ca$_V$1.3 channels. Maps were rendered at 5 nm, the pixel size for the images presented. BK-positive pixels formed multi-pixel aggregates, which has been interpreted as homo-clusters of

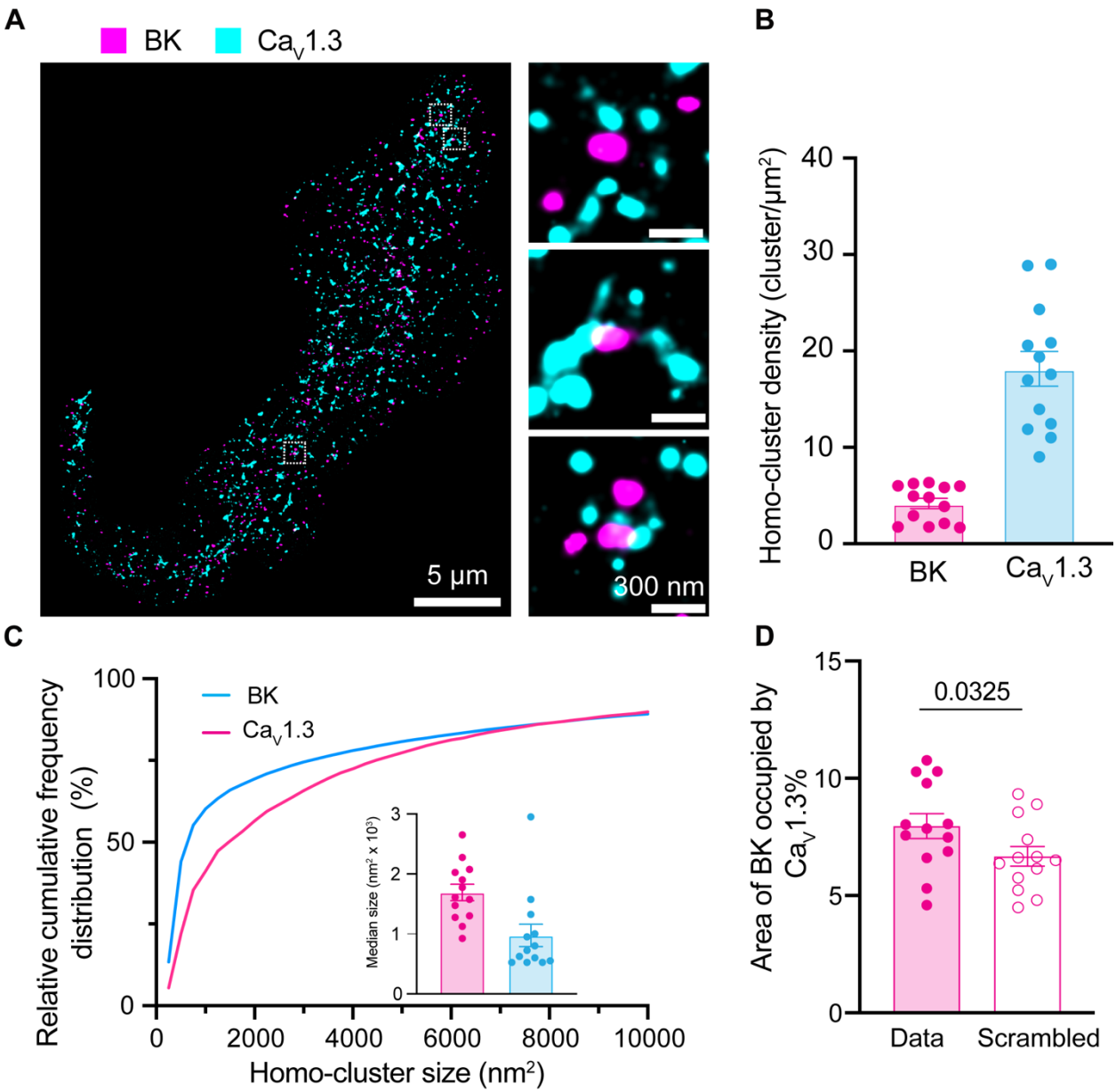

Figure 8. Formation of BK and Ca$_V$1.3 hetero-clusters in INS-1 cells. A. Representative localization map of antibodies against BK (magenta) and Ca$_V$1.3 (cyan) channels. Magnifications are shown in the insets on the right. **B.** Scatter dot plot of homo-cluster densities of BK and Ca$_V$1.3 channels in INS-1 cells. **C.** Cumulative frequency distributions of homo-cluster sizes of BK and Ca$_V$1.3 channels. Inset compares median size of BK and Ca$_V$1.3 homo-clusters. **D.** Comparison of colocalization between BK and Ca$_V$1.3 and between scrambled BK and Ca$_V$1.3. Data points are from n = 13 cells. Scale bar is 5 µm and 300 nm in the magnifications.

BK channels. Ca$_V$1.3 channels also formed homo-clusters. When looking at the formation of BK and Ca$_V$1.3 hetero-clusters, no fixed geometry or stoichiometry was observed. On the contrary, maps showed a distribution of distances between BK and Ca$_V$1.3 detected pixels. In some cases, BK and Ca$_V$1.3 channels were perfectly

overlapping, as if the detection of the antibodies could not be separated by the 20 nm resolution. In other cases, BK and Ca_V1.3 channels were adjacent (less than 5 nm), and in other cases, BK homo-clusters were surrounded by a variable number of Ca_V1.3 channels.

To provide a more quantitative description of the maps, we measured cluster density, cluster size, and colocalization. We used the particle analysis tool of the software ImageJ for these measurements. In this analysis, a particle for represents positive pixels irrespective of the number of pixels composed. As a note, a particle of one pixel would likely to be a single channel, whereas a particle composed of many pixels would likely to be a cluster of channels. INS-1 cells showed 4 times as many Ca_V1.3 particles as BK particles (Figure 8B). Figure 8C shows the frequency distribution of particle size, where the median area is 1691 nm^2 for BK and 975 nm^2 for Ca_V1.3. We also found 7.5% colocalization between BK and Ca_V1.3 particles (Figure 8D), which was higher than the colocalization calculated using scrambled images.

Hetero-clusters of BK and Ca_V1.3 channels are detected at the plasma membrane soon after their expression.

In light of our results, our current model is that BK and Ca_V1.3 hetero-clusters form prior to their insertion into the plasma membrane. One prediction based on this model is that channels inserted in the plasma membrane would appear as hetero-clusters already at early time points after the start of their synthesis. To test this prediction, we transfected tsA-201 cells with BK and Ca_V1.3 channels and performed a chase experiment to detect their presence at the plasma membrane using super-resolution microscopy. We measured particle size, density, and colocalization at 18, 24, and 48 hours after transfection. Notably, although the channels were transfected simultaneously, BK particles were detected in the plasma membrane 18 hours after transfection, whereas Ca_V1.3 particles were detected 24 hours after transfection (Figure 9A-C). The distribution of BK and Ca_V1.3 particle size did not change with the time after transfection (Figure 9D and E), in agreement with Sato et al., 2019 [24].

In support of our prediction, we found particles of Ca_V1.3 near BK particles as soon as the expression of Ca_V1.3 channels was detected in the plasma membrane (24 hours after transfection, enlarged Figure 9B). To test this hypothesis further, we compared plots of localization preference at 24 and 48 hours. These plots were constructed by measuring the percentage of Ca_V1.3 area occupying concentric regions of 20 nm width around BK particles. Values were normalized to the percentage of colocalization found at

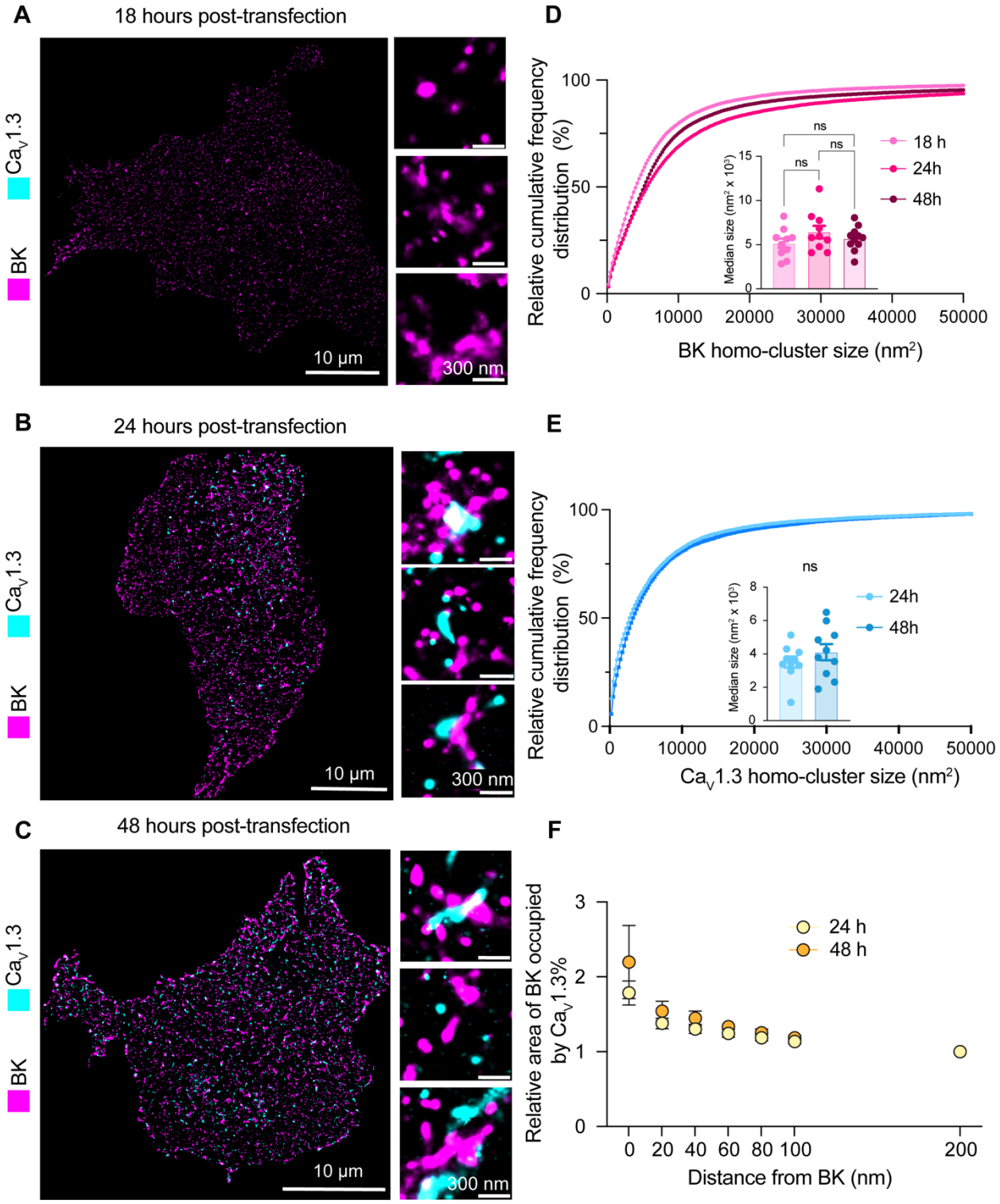

Figure 9. Hetero-clusters of BK and Ca$_V$1.3 channels are detected at the plasma membrane soon after their expression begins. A-C. Representative localization maps of antibodies against BK and Ca$_V$1.3 channels. (A) 18 hours, (B) 24 hours, or (C) 48 hours after DNA transfection into cells. Enlargements are shown in insets. **D.** Cumulative frequency distributions of BK homo-cluster size at 18, 24, and 48 hours. Inset compares median BK homo-cluster areas. **E.** Cumulative frequency distributions of Ca$_V$1.3 homo-clusters at 24 and 48 hours. Inset compares median Ca$_V$1.3 cluster areas. Ca$_V$1.3 clusters are not present at the 18-hour time point. **F.** Comparison of colocalization plots between BK and Ca$_V$1.3 channels at 24 and 48-hour time points. Data points are from n = 10 cells. Scale bar is 10 µm and 300 nm in enlargements.

200 nm from BK. Figure 9F shows that the localization preference plots are identical at 24 and 48 hours, consistent with the hypothesis that both channels are inserted together into the plasma membrane already as hetero-clusters.

Discussion

Intracellular Assembly of BK and Ca_V1.3 Channels

Previous work from our group has revealed the organization of hetero-clusters of large-conductance calcium-activated potassium (BK) channels and voltage-gated calcium channels, particularly Ca_V1.3, within nanodomains. This spatial organization is crucial for the functional coupling that enables BK channels to respond promptly to calcium influx, thereby modulating cellular excitability [15]. While physical details of BK-Ca_V1.3 interactions are not fully elucidated, the evidence suggests that BK channels interact with both the Ca_V α1 subunit and its auxiliary subunits [34, 35]. Our findings highlight the intracellular assembly of BK-Ca_V1.3 hetero-clusters, though limitations in resolution and organelle-specific analysis prevent precise quantification of the proportion of intracellular complexes that ultimately persist on the cell surface. While our data confirms that hetero-clusters form before reaching the plasma membrane, it remains unclear whether all intracellular hetero-clusters transition intact to the membrane or undergo rearrangement or disassembly upon insertion. Future studies utilizing live cell tracking and high resolution imaging will be valuable in elucidating the fate and stability of these complexes after membrane insertion.

A stochastic model of ion channel homo-cluster formation in the plasma membrane proposes that random yet probabilistic interactions between ion channels contribute to their formation [24]. These clusters are stabilized and organized within specific membrane regions through biophysical mechanisms such as membrane curvature. Recent findings on spatial organization of G-protein coupled receptors provide additional support for this framework, demonstrating that the coupling of membrane proteins to the curvature of the plasma membrane acts as a driving force for their clustering into functional domains [36]. Yet, the mechanisms regulating the spatial organization of hetero-clusters are less known.

Colocalization and Trafficking Dynamics

The colocalization of BK and Ca_V1.3 channels in the ER and at ER exit sites before reaching the Golgi suggests a coordinated trafficking mechanism that facilitates the formation of multi-channel complexes crucial for calcium signaling and membrane excitability [37, 38]. Given the distinct roles of these compartments,

colocalization at the ER and ER exit sites may reflect transient proximity rather than stable interactions. Their presence in the Golgi further suggests that post-translational modifications and additional assembly steps occur before plasma membrane transport, providing further insight into hetero-cluster maturation and sorting events. By examining BK-Ca_V1.3 hetero-cluster distribution across these trafficking compartments, we ensure that observed colocalization patterns are considered within a broader framework of intracellular transport mechanisms [39]. Previous studies indicate that ER exit sites exhibit variability in cargo retention and sorting efficiency [40], emphasizing the need for careful evaluation of colocalization data. Accounting for these complexities allows for a robust assessment of signaling complexes formation and trafficking pathways.

BK Surface Expression and Independent Trafficking Pathways

BK surface expression in the absence of Ca_V1.3 indicates that its trafficking does not strictly rely on Ca_V1.3-mediated interactions. Since BK channels can be activated by multiple calcium sources, their presence in intracellular compartments suggests that their surface expression is governed by intrinsic trafficking mechanisms rather than direct calcium-dependent regulation. While some BK and Ca_V1.3 hetero-clusters assemble into signaling complexes intracellularly, other BK channels follow independent trafficking pathways, demonstrating that complex formation is not obligatory for all BK channels. Differences in their transport kinetics further reinforce the idea that their intracellular trafficking is regulated through distinct mechanisms. Studies have shown that BK channels can traffic independently of Ca_V1.3, relying on alternative calcium sources for activation [13, 41]. Additionally, Ca_V1.3 exhibits slower synthesis and trafficking kinetics than BK, emphasizing that their intracellular transport may not always be coordinated. These findings suggest that BK and Ca_V1.3 exhibit both independent and coordinated trafficking behaviors, influencing their spatial organization and functional interactions.

mRNA Colocalization and Protein Trafficking

The colocalization of mRNAs encoding BK and Ca_V1.3 channels suggests a coordinated translation mechanism that facilitates their proximal synthesis and subsequent assembly into functional complexes. As a mechanism, mRNA localization enhances protein enrichment at functional sites, coordinating with translational control to position ion channels at specific subcellular domains; ion channel positioning is especially critical for neurons and cardiomyocytes [42, 43]. By

synthesizing these channels in close proximity, channels can be efficiently assembled into functional units, making this process crucial for precise targeting and trafficking of ion channels to specific subcellular domains, thereby ensuring proper cellular function and efficient signal transduction [42, 44-46]. Disruption in mRNA localization or protein trafficking can lead to ion channel mislocalization, resulting in altered cellular function and disease [47, 48]. In cardiac cells, precise trafficking of ion channels to specific membrane subdomains is crucial for maintaining normal electrical and mechanical functions, and its disruption contributes to heart disease and arrhythmias [32, 49, 50] Similarly, in neurons, the localization and translation of mRNA at synaptic sites are essential for synaptic plasticity, and disturbances can lead to neurological disorders [51, 52].

Co-translational Regulation and Functional Coordination

The co-translational association of transcripts encoding BK and Ca_V1.3 ion channels, as well as other known calcium sources like RyR2, may serve as a mechanism to ensure the precise stoichiometry and assembly of functional channel complexes. This precise assembly is also critical for spatially organizing RyR2 and BK channels, as shown in airway myocytes, where the proximity of these channels underlies the efficient activation of BK channels by localized Ca^{2+} sparks [32]. Co-translational association of transcripts encoding K_V1.3 channels was the first example in which the interaction of nascent K_V1.3 N-termini facilitates proper tertiary and quaternary structure required for oligomerization [53, 54]. Similarly, co-translational heteromeric association of hERG1a and hERG1b subunits ensures that cardiac IK_r currents exhibit the appropriate biophysical properties and magnitude necessary for normal ventricular action potential shaping [45]. The precise mechanism by which BK transcripts are associated with the transcripts of calcium sources like Ca_V1.3 and RyR2 channels remain to be elucidated. While it is conceivable that complementary base pairing or tertiary structural interactions play a role, RNA binding proteins (RBPs) are likely key mediators of these associations.

Conclusion and Future Directions

This study provides novel insights into the organization of BK and Ca_V1.3 channels in hetero-clusters, emphasizing their assembly within the ER, at ER exit sites, and within the Golgi. Our findings suggest that BK and Ca_V1.3 channels begin assembling intracellularly before reaching the plasma membrane, shaping their spatial organization, and potentially facilitating functional coupling. While this suggests a

coordinated process that may contribute to functional coupling, further investigation is needed to determine the extent to which these hetero-clusters persist upon membrane insertion. While our study advances the understanding of BK and Ca_V1.3 hetero-cluster assembly, several key questions remain unanswered. What molecular machinery drives this colocalization at the mRNA and protein level? How do disruptions to complex assembly contribute to channelopathies and related diseases? Additionally, a deeper investigation into the role of RNA binding proteins in facilitating transcript association and localized translation is warranted.

Acknowledgments

We thank Gail Robertson for her immense support and influence in designing and conducting this project. We thank Alexey Merz for his support and feedback through this project. We thank Bertil Hille for his contribution to editing the writing of this project. We thank Martina Hunt, Maria Elena Danoviz, Paula Martinez-Feduchi, Wendy Piñon-Teal, and Raul Riquelme for reading and providing feedback on the manuscript. We thank William Catterall and Ruth E. Westenbroek for providing the antibody against Ca_V1.3. This study was supported by the National Institutes of Health MIRA R35 GM142690 to O.V. C.M. was supported by HL162609 and the Freeman Hrabowski HHMI Scholars program.

Supplementary figures

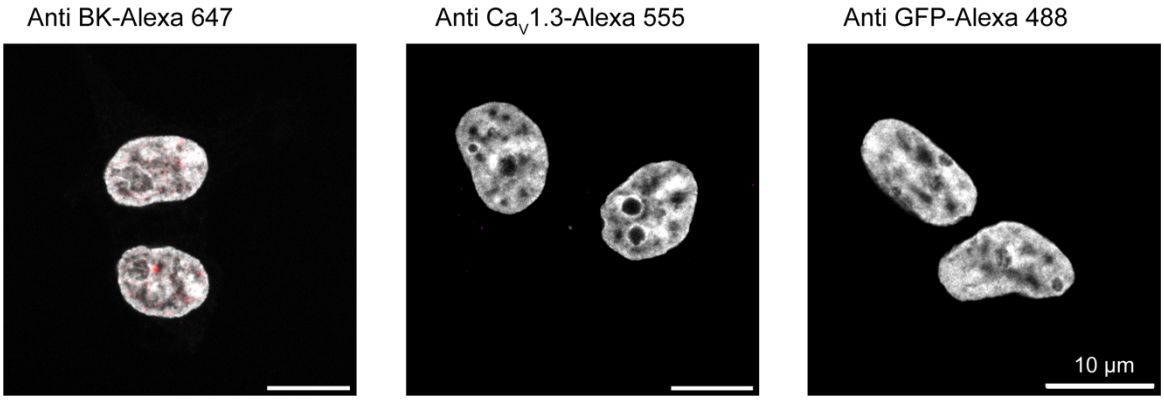

Figure 2-Supplementary 1. Validation of antibodies against BK, Ca_V1.3 and GFP. Representative confocal images of tsA-201 cells immuno-tested for BK channels (left), Ca_V1.3 channels (middle), and GFP proteins (right). Cells were not transfected. Nuclei were stained with DAPI and pseudo colored in gray. Scale bar is 10 µm for all images.

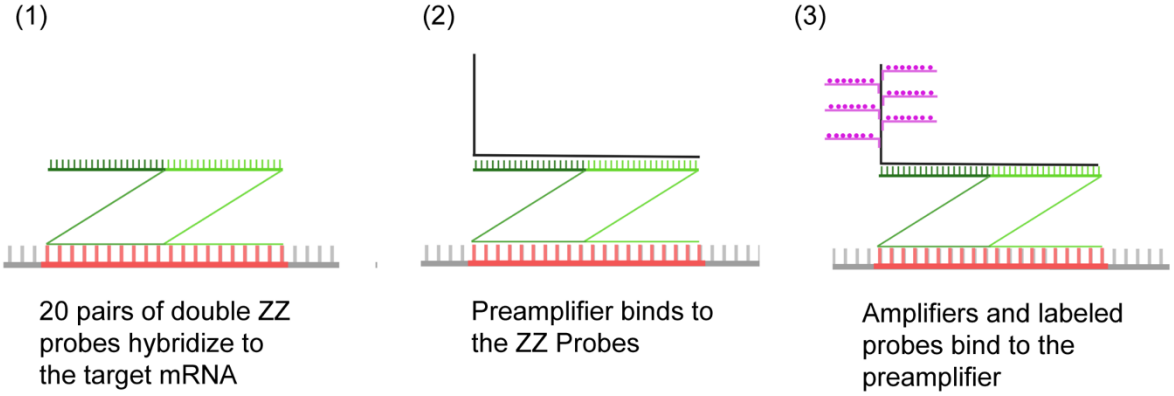

Figure 5-Supplementary 1. Illustration of RNA scope methodology. Steps to detect an mRNA sequence (red zipper) consisting of (1) hybridization, (2) pre-amplification, (3) and labeling. Double ZZ probes are shown in green. Dye labeling the mRNA is shown in magenta.

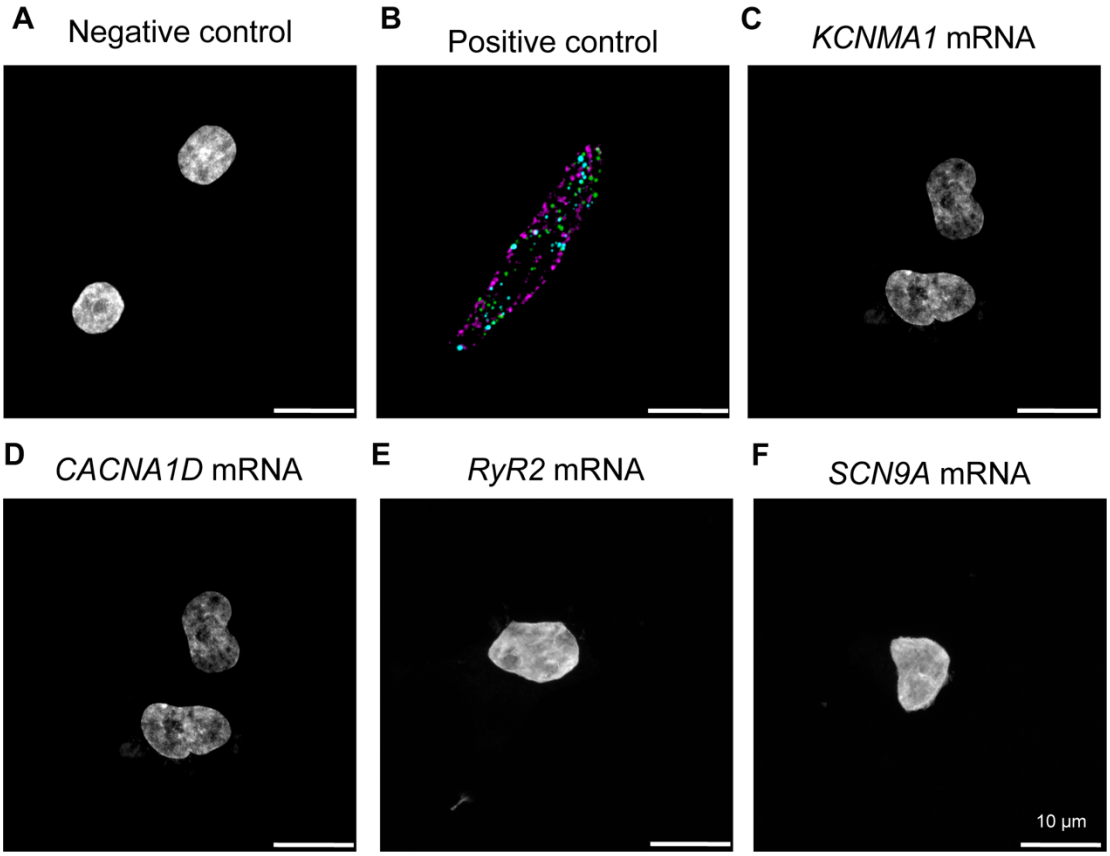

Figure 5-Supplementary 2. RNA probe validation. A. Representative images of INS-1 cells subjected to mRNA probes against a bacterial gene (DapB from *Bacillus subtilis*). **B.** Representative images of INS-1 cells subjected to mRNA probes against three constitutive mammalian genes (ubiquitin C, cyclophilin B, and a polymerase II subunit). **C - F** show tsA-201 cells that were naive to exogenous DNA but treated with mRNA probes against the genes for (**C**) BK channels, (**D**) Ca_V1.3 channels, (**E**) Ryanodine Receptors type 2 (RyR2), and (**F**) Na_V1.7 channels. Scale bar is 10 µm.

Key Resources Table

Reagent type	Designation	Source	Identifiers	Additional info.
Cell line	tsA-201	Sigma	RRID:CVCL_2737	
Cell line	INS-1	Sigma	RRID:CVCL_0352	
DNA clone	CaV1.3	Addgene	RRID:SCR_002037	Addgene ID: 49333
DNA clone	Slo1 (BK)	Addgene	RRID:SCR_002037	Addgene ID: 113566
DNA clone	KDEL-mox-GFP	Addgene	RRID:SCR_002037	Addgene ID: 68072
DNA clone	pmGFP-Sec16	Addgene	RRID:SCR_002037	Addgene ID: 15775
DNA clone	Golgi mGFP	Addgene	RRID:SCR_002037	Addgene ID: 182877
DNA clone	pPH-PLC-δ-GFP	Addgene	RRID:SCR_002037	Addgene ID: 51407
DNA clone	CaVβ3	Diane Lipscombe, Brown University		Auxiliary subunits for CaV1.3
DNA clone	CaVα2δ1	Diane Lipscombe, Brown University		Auxiliary subunits for CaV1.3
Genetic reagent	RNAscope 3-plex Positive Control Probes	Advanced Cell Diagnostics		Cat. No. 320871
Genetic reagent	RNAscope 3-plex Negative Control Probes	Advanced Cell Diagnostics		Cat. No. 320871
Genetic reagent	RNAscope™ Probe- Rn-Ryr	Advanced Cell Diagnostics		Cat. No. 2560931
Genetic reagent	RNAscope™ Probe- Rn-Scn9a	Advanced Cell Diagnostics		Cat. No. 317851

Genetic reagent	RNAscope Probe- Rn-Kcnma1-C3	Advanced Cell Diagnostics		Cat. No. 1108261-C3
Genetic reagent	RNAscope Probe- Rn-Cacna1d-C2	Advanced Cell Diagnostics		Cat. No. 409361-C2
Genetic reagent	RNAscope Probe- Rn-Gapdh	Advanced Cell Diagnostics		Cat. No. 409821
Antibody	Anti-CaV1.3	Drs. William Catterall and Ruth Westenbroek		rabbit primary antibody recognizing the residues 809 to 825 located at the intracellular II-III loop of the channel (DNKVTIDDYQEEAEDKD)
Antibody	Anti-Slo1	Millipore Sigma	RRID:AB_10805948	mouse monoclonal antibody clone L6/60, Cat. No. MABN70
Antibody	Anti GFP	abcam	RRID:AB_305643	corresponding to recombinant full length protein corresponding to *Aequorea victoria* GFP, Cat. No. ab6673
Antibody	Anti-58K Golgi	abcam	RRID:AB_2107005	Cat. No. ab27043
Antibody	Donkey anti-mouse-Alexa 647	Invitrogen	RRID:AB_2536183	Cat. No. A-31573
Antibody	Donkey anti-rabbit-Alexa 555	Invitrogen	RRID:AB_2534017	Cat. No. A10042
Antibody	Donkey anti-goat-Alexa 488	Invitrogen	RRID:AB_162542	Cat. No. A-31571
Antibody	Duolink® In Situ PLA® probe anti-rabbit PLUS	Sigma	RRID:AB_2810940	

Antibody	Duolink® In Situ PLA® probe anti-mouse PLUS	Sigma	RRID:AB_2810939	
Commercial assay or kit	Duolink® In Situ Red Starter Kit	Sigma		Cat. No. DUO92008
Recombinant DNA reagent	Lipofectamine 3000	Invitrogen	RRID:L30000	
Reagent	ProLong™ Gold Antifade Mountant with DAPI	Invitrogen		Cat. No. P36931
Commercial assay or kit	RNAscope™ Multiplex Fluorescent V2 Assay	Advanced Cell Diagnostics		Cat. No. 323270
Software, algorithm	Prism	GraphPad	RRID:SCR_002798	
Software, algorithm	Excel	Microsoft		
Software, algorithm	ImageJ	NIH	RRID:SCR_003070	
Software, algorithm	NImOS software	ONI		v.1.18.3

References:

1. Contreras, G.F., et al., *A BK (Slo1) channel journey from molecule to physiology.* Channels (Austin), 2013. **7**(6): p. 442-58.
2. Kaczorowski, G.J., et al., *High-conductance calcium-activated potassium channels; structure, pharmacology, and function.* J Bioenerg Biomembr, 1996. **28**(3): p. 255-67.
3. Contet, C., et al., *BK Channels in the Central Nervous System.* Int Rev Neurobiol, 2016. **128**: p. 281-342.
4. Ancatén-González, C., et al., *Ca2+- and Voltage-Activated K+ (BK) Channels in the Nervous System: One Gene, a Myriad of Physiological Functions.* Int J Mol Sci, 2023. **24**(4).
5. Dopico, A.M., A.N. Bukiya, and J.H. Jaggar, *Calcium- and voltage-gated BK channels in vascular smooth muscle.* Pflugers Arch, 2018. **470**(9): p. 1271-1289.
6. Hu, S.L., H.S. Kim, and A.Y. Jeng, *Dual action of endothelin-1 on the Ca2(+)-activated K+ channel in smooth muscle cells of porcine coronary artery.* Eur J Pharmacol, 1991. **194**(1): p. 31-6.
7. Semenov, I., et al., *BK channel beta1-subunit regulation of calcium handling and constriction in tracheal smooth muscle.* Am J Physiol Lung Cell Mol Physiol, 2006. **291**(4): p. L802-10.
8. Dupont, C., et al., *BK channels promote action potential repolarization in skeletal muscle but contribute little to myotonia.* Pflugers Arch, 2024. **476**(11): p. 1693-1702.
9. Pallotta, B.S., K.L. Magleby, and J.N. Barrett, *Single channel recordings of Ca2+-activated K+ currents in rat muscle cell culture.* Nature, 1981. **293**(5832): p. 471-4.
10. Meredith, A.L., *BK Channelopathies andand KCNMA1-Linked Disease Models.* Annu Rev Physiol, 2024. **86**: p. 277-300.
11. Bailey, C.S., et al., *KCNMA1-linked channelopathy.* J Gen Physiol, 2019. **151**(10): p. 1173-1189.
12. Houamed, K.M., I.R. Sweet, and L.S. Satin, *BK channels mediate a novel ionic mechanism that regulates glucose-dependent electrical activity and insulin secretion in mouse pancreatic beta-cells.* J Physiol, 2010. **588**(Pt 18): p. 3511-23.
13. Shah, K.R., X. Guan, and J. Yan, *Structural and Functional Coupling of Calcium-Activated BK Channels and Calcium-Permeable Channels Within Nanodomain Signaling Complexes.* Front Physiol, 2021. **12**: p. 796540.

14. Berkefeld, H., et al., *BKCa-Cav channel complexes mediate rapid and localized Ca2+-activated K+ signaling.* Science, 2006. **314**(5799): p. 615-20.
15. Vivas, O., et al., *Proximal clustering between BK and CaV1.3 channels promotes functional coupling and BK channel activation at low voltage.* Elife, 2017. **6**.
16. Prakriya, M. and C.J. Lingle, *Activation of BK channels in rat chromaffin cells requires summation of Ca(2+) influx from multiple Ca(2+) channels.* J Neurophysiol, 2000. **84**(3): p. 1123-35.
17. Lipscombe, D., T.D. Helton, and W. Xu, *L-type calcium channels: the low down.* J Neurophysiol, 2004. **92**(5): p. 2633-41.
18. Chen, G., et al., *BK channel modulation by positively charged peptides and auxiliary γ subunits mediated by the Ca2+-bowl site.* Journal of General Physiology, 2023. **155**(6).
19. Liu, F., et al., *Cotranslational association of mRNA encoding subunits of heteromeric ion channels.* Proc Natl Acad Sci U S A, 2016. **113**(17): p. 4859-64.
20. Eichel, C.A., et al., *A microtranslatome coordinately regulates sodium and potassium currents in the human heart.* eLife, 2019. **8**: p. e52654.
21. Yang, S., et al., *Membrane curvature governs the distribution of Piezo1 in live cells.* Nature Communications, 2022. **13**(1): p. 7467.
22. Chen, Z., et al., *EMC chaperone–CaV structure reveals an ion channel assembly intermediate.* Nature, 2023. **619**(7969): p. 410-419.
23. Cheng, E.P., et al., *Restoration of Normal L-Type Ca2+ Channel Function During Timothy Syndrome by Ablation of an Anchoring Protein.* Circulation Research, 2011. **109**(3): p. 255-261.
24. Sato, D., et al., *A stochastic model of ion channel cluster formation in the plasma membrane.* J Gen Physiol, 2019. **151**(9): p. 1116-1134.
25. Eichel, C.A., et al., *A microtranslatome coordinately regulates sodium and potassium currents in the human heart.* Elife, 2019. **8**.
26. Lu, J., et al., *T1-T1 interactions occur in ER membranes while nascent Kv peptides are still attached to ribosomes.* Biochemistry, 2001. **40**(37): p. 10934-46.
27. Hell, J.W., et al., *Identification and differential subcellular localization of the neuronal class C and class D L-type calcium channel alpha 1 subunits.* J Cell Biol, 1993. **123**(4): p. 949-62.
28. Costantini, L.M., et al., *A palette of fluorescent proteins optimized for diverse cellular environments.* Nat Commun, 2015. **6**: p. 7670.

29. Georgiades, P., et al., *The flexibility and dynamics of the tubules in the endoplasmic reticulum.* Sci Rep, 2017. **7**(1): p. 16474.
30. Nixon-Abell, J., et al., *Increased spatiotemporal resolution reveals highly dynamic dense tubular matrices in the peripheral ER.* Science, 2016. **354**(6311).
31. Bashour, A.M. and G.S. Bloom, *58K, a microtubule-binding Golgi protein, is a formiminotransferase cyclodeaminase.* J Biol Chem, 1998. **273**(31): p. 19612-7.
52. Lifshitz, L.M., et al., *Spatial organization of RYRs and BK channels underlying the activation of STOCs by Ca(2+) sparks in airway myocytes.* J Gen Physiol, 2011. **138**(2): p. 195-209.
33. Anderson, C.L., et al., *Most LQT2 mutations reduce Kv11.1 (hERG) current by a class 2 (trafficking-deficient) mechanism.* Circulation, 2006. **113**(3): p. 365-73.
34. Rehak, R., et al., *Low voltage activation of KCa1.1 current by Cav3-KCa1.1 complexes.* PLoS One, 2013. **8**(4): p. e61844.
35. Zhang, F.X., et al., *BK Potassium Channels Suppress Cavα2δ Subunit Function to Reduce Inflammatory and Neuropathic Pain.* Cell Rep, 2018. **22**(8): p. 1956-1964.
36. Kockelkoren, G., et al., *Molecular mechanism of GPCR spatial organization at the plasma membrane.* Nat Chem Biol, 2024. **20**(2): p. 142-150.
37. Berkefeld, H., B. Fakler, and U. Schulte, Ca2+-activated K+ channels: from protein complexes to function. Physiol Rev, 2010. 90(4): p. 1437-59.
38. Loane, D.J., P.A. Lima, and N.V. Marrion, Co-assembly of N-type Ca2+ and BK channels underlies functional coupling in rat brain. J Cell Sci, 2007. 120(Pt 6): p. 985-95.
39. Boncompain, G. and F. Perez, *The many routes of Golgi-dependent trafficking.* Histochemistry and Cell Biology, 2013. **140**(3): p. 251-260.
40. Kurokawa, K. and A. Nakano, *The ER exit sites are specialized ER zones for the transport of cargo proteins from the ER to the Golgi apparatus.* The Journal of Biochemistry, 2019. **165**(2): p. 109-114.
41. Chen, A.L., et al., Calcium-Activated Big-Conductance (BK) Potassium Channels Traffic through Nuclear Envelopes into Kinocilia in Ray Electrosensory Cells. Cells, 2023. 12(17): p. 2125.
42. Vacher, H., D.P. Mohapatra, and J.S. Trimmer, *Localization and targeting of voltage-dependent ion channels in mammalian central neurons.* Physiol Rev, 2008. **88**(4): p. 1407-47.
43. Medioni, C., K. Mowry, and F. Besse, *Principles and roles of mRNA localization in animal development.* Development, 2012. **139**(18): p. 3263-76.

44. Blandin, C.E., et al., *Remodeling of Ion Channel Trafficking and Cardiac Arrhythmias.* Cells, 2021. **10**(9).
45. Dai, G., *Signaling by Ion Channels: Pathways, Dynamics and Channelopathies.* Mo Med, 2023. **120**(5): p. 367-373.
46. Jameson, M.B., et al., *Pairwise biosynthesis of ion channels stabilizes excitability and mitigates arrhythmias.* Proc Natl Acad Sci U S A, 2023. **120**(42): p. e2305295120.
47. Wang, E.T., et al., *Dysregulation of mRNA Localization and Translation in Genetic Disease.* The Journal of Neuroscience, 2016. **36**(45): p. 11418.
48. Wang, J., et al., *RNA trafficking and subcellular localization—a review of mechanisms, experimental and predictive methodologies.* Briefings in Bioinformatics, 2023. **24**(5): p. bbad249.
49. Smyth, J.W. and R.M. Shaw, *Forward trafficking of ion channels: what the clinician needs to know.* Heart Rhythm, 2010. **7**(8): p. 1135-40.
50. Basheer, W.A. and R.M. Shaw, *Connexin 43 and CaV1.2 Ion Channel Trafficking in Healthy and Diseased Myocardium.* Circ Arrhythm Electrophysiol, 2016. **9**(6): p. e001357.
51. Eliscovich, C., S.M. Shenoy, and R.H. Singer, *Imaging mRNA and protein interactions within neurons.* Proc Natl Acad Sci U S A, 2017. **114**(10): p. E1875-E1884.
52. Yoon, Y.J., et al., *Glutamate-induced RNA localization and translation in neurons.* Proc Natl Acad Sci U S A, 2016. **113**(44): p. E6877-E6886.
53. Robinson, J.M. and C. Deutsch, *Coupled tertiary folding and oligomerization of the T1 domain of Kv channels.* Neuron, 2005. **45**(2): p. 223-32.
54. Tu, L. and C. Deutsch, *Evidence for dimerization of dimers in K+ channel assembly.* Biophys J, 1999. **76**(4): p. 2004-17.